

ARPES study of Y_2O_2Bi single crystals: Intrinsic electronic structure of Bi square nets

Yun-Bo Wu(吴云波), Tong-Rui Li(李彤瑞), Zhi-Peng Cao(曹志鹏), Zhan-Feng Liu(刘站锋), Yu-Liang Li(李昱良), Zheng-Ming Shang(尚政明), Xin Zheng(郑新), Hui Tian(田慧), Zong-Yi Wang(王宗一), Yu-Tong Bi(毕雨桐), Hao-Yang Zhou(周浩洋), Yi Liu(刘毅), Guo-Bin Zhang(张国斌), Zheng-Tai Liu(刘正太), Da-Wei Shen(沈大伟), Li-Dong Zhang(张李东), Sheng-Tao Cui(崔胜涛), and Zhe Sun(孙喆)
Citation: Chin. Phys. B, 2026, 35 (**4**): 047101. DOI: 10.1088/1674-1056/ae04d9
http://cpb.iphy.ac.cn; http://iopscience.iop.org/cpb

What follows is a list of articles you may be interested in

Two-dimensional kagome semiconductor $Sc_6S_5X_6$ (X = Cl, Br, I) with trilayer kagome lattice

Jin-Ling Yan(闫金铃), Xing-Yu Wang(王星雨), Gen-Ping Wu(吴根平), Hao Wang(王浩), Ya-Jiao Ke(柯亚娇), Jiafu Wang(王嘉赋), Zhi-Hong Liu(刘志宏), and Jun-Hui Yuan(袁俊辉)
Chin. Phys. B, 2026, 35 (**2**): 027102. DOI: 10.1088/1674-1056/ae00b4

Unique high-energy excitons in two-dimensional transition metal dichalcogenides

Yongsheng Gao(高永盛), Yuanzheng Li(李远征), Weizhen Liu(刘为振), Chuxin Yan(闫楚欣), Qingbin Wang(王庆彬), Wei Xin(辛巍), Haiyang Xu(徐海阳), and Yichun Liu(刘益春)
Chin. Phys. B, 2025, 34 (**9**): 097102. DOI: 10.1088/1674-1056/ade074

Anomalous ultrafast thermalization of photoexcited carriers in two-dimensional materials induced by orbital coupling

Zhuoqun Wen(文卓群), Haiyu Zhu(诸海渝), Wen-Hao Liu(刘文浩), Zhi Wang(王峙), Wen Xiong(熊稳), and Xingzhan Wei(魏兴战)
Chin. Phys. B, 2025, 34 (**7**): 077103. DOI: 10.1088/1674-1056/adc191

Unveiling the thermal transport mechanisms in novel carbon-based graphene-like materials using machine-learning potential

Yao-Yuan Zhang(章耀元), Meng-Qiu Long(龙孟秋), Sai-Jie Cheng(程赛杰), and Wu-Xing Zhou(周五星)
Chin. Phys. B, 2025, 34 (**6**): 067101. DOI: 10.1088/1674-1056/adca18

High-temperature ferromagnetism and strong π-conjugation feature in two-dimensional manganese tetranitride

Ming Yan(闫明), Zhi-Yuan Xie(谢志远), and Miao Gao(高淼)
Chin. Phys. B, 2023, 32 (**3**): 037104. DOI: 10.1088/1674-1056/acae7b

---

ARPES study of Y_2O_2Bi single crystals: Intrinsic electronic structure of Bi square nets

Yun-Bo Wu(吴云波)[1,†], Tong-Rui Li(李彤瑞)[1,†], Zhi-Peng Cao(曹志鹏)[2], Zhan-Feng Liu(刘站锋)[1], Yu-Liang Li(李昱良)[1], Zheng-Ming Shang(尚政明)[1], Xin Zheng(郑新)[1], Hui Tian(田慧)[1], Zong-Yi Wang(王宗一)[1], Yu-Tong Bi(毕雨桐)[1], Hao-Yang Zhou(周浩洋)[1], Yi Liu(刘毅)[1], Guo-Bin Zhang(张国斌)[1], Zheng-Tai Liu(刘正太)[3,4], Da-Wei Shen(沈大伟)[1], Li-Dong Zhang(张李东)[1], Sheng-Tao Cui(崔胜涛)[1,‡], and Zhe Sun(孙喆)[1,5,6,7,§]

[1] *National Synchrotron Radiation Laboratory, University of Science and Technology of China, Hefei* 230029, *China*
[2] *Key Laboratory of Quantum Materials and Devices of Ministry of Education, School of Physics, Southeast University, Nanjing* 211189, *China*
[3] *Shanghai Synchrotron Radiation Facility, Shanghai Advanced Research Institute, Chinese Academy of Sciences, Shanghai* 201210, *China*
[4] *National Key Laboratory of Materials for Integrated Circuits, Shanghai Institute of Microsystem and Information Technology, Chinese Academy of Sciences, Shanghai* 200050, *China*
[5] *Department of Physics, CAS Key Laboratory of Strongly-coupled Quantum Matter Physics, University of Science and Technology of China, Hefei* 230026, *China*
[6] *Zhejiang Institute of Photoelectronics, Jinhua* 321004, *China*
[7] *Collaborative Innovation Center of Advanced Microstructures, Nanjing* 210093, *China*

(Received 31 July 2025; revised manuscript received 28 August 2025; accepted manuscript online 9 September 2025)

The Bi square net, a structural motif in a diverse array of layered compounds, has emerged as a desirable system for investigating the interplay between strong spin–orbit coupling, reduced dimensionality, and magnetism. We present a comprehensive study of Y_2O_2Bi single crystals using high-resolution angle-resolved photoemission spectroscopy (ARPES) and density functional theory (DFT) calculations to elucidate the intrinsic electronic structure of the Bi square net. Our findings reveal a pronounced two-dimensional character of the electronic states, with the Bi square net dominating the low-energy electronic structure. While Y_2O_2Bi itself exhibits no topological features, DFT calculations on related Bi square net compounds reveal that the surrounding crystal environment can induce non-trivial topology, as exemplified by the topological insulator LiBi. This comparative study establishes a crucial benchmark for understanding Bi square net physics and informs the design of future Bi square net-based quantum materials.

Keywords: two-dimensional materials, electronic structure, Bi square net, spin–orbit coupling

PACS: 71.20.–b, 71.70.Ej, 73.20.At, 74.25.Jb

DOI: 10.1088/1674-1056/ae04d9 **CSTR:** 32038.14.CPB.ae04d9

1. Introduction

The discovery and design of novel quantum materials are crucial for advancing both fundamental scientific understanding and technological innovation.[1–4] In recent years, two-dimensional (2D) materials have emerged as a particularly promising avenue for exploring novel quantum phenomena. The reduced dimensionality of 2D materials provides a unique platform for manipulating and enhancing electronic interactions.[5–14] Among these materials, systems containing nets of heavy elements, particularly bismuth, offer a rich playground for investigating novel electronic states due to the strong influence of spin–orbit coupling (SOC).[15–17] The RE_2O_2Bi family (RE = rare-earth elements) represents a particularly intriguing class of materials in this context. These compounds feature a layered structure in which electrically conductive Bi square nets are sandwiched between insulating $[RE_2O_2]^{2+}$ layers.[18,19] This structure effectively isolates the Bi square net, making it an ideal system for studying its intrinsic properties.

The Bi square net plays a significant role in a variety of exotic phenomena observed in related materials. Analogous to the carbon honeycomb lattice in graphene, the Bi square net provides a unique environment for the emergence of novel electronic states. For example, in AMnBi$_2$ (A = Sr, Ca), these nets host highly anisotropic Dirac fermions.[20,21] In EuMnBi$_2$, the Bi square net exhibits a fascinating interplay between magnetism and electronic structure.[22] In $CeNi_{0.8}Bi_2$, the electronic states of the Bi square net are responsible for superconductivity.[23] Recent studies on RE_2O_2Bi compounds have revealed several intriguing properties, including the emergence of superconductivity at low temperatures in compounds with heavy rare-earth elements upon excess oxygen incorporation.[24–27] Theoretical calculations suggest that the large SOC in these materials suppresses charge density wave instabilities, a phenomenon rarely observed in 2D

[†]These authors contributed equally to this work.
[‡]Corresponding author. E-mail: shengtaocui@ustc.edu.cn
[§]Corresponding author. E-mail: zsun@ustc.edu.cn

© 2026 Chinese Physical Society and IOP Publishing Ltd. All rights, including for text and data mining, AI training, and similar technologies, are reserved.

systems.[28,29] These diverse observations highlight the complex interplay of factors governing the electronic properties of Bi nets and their influence on macroscopic material behavior. Despite these exciting developments, a comprehensive understanding of the intrinsic electronic structure of the Bi square net has remained elusive. The challenge lies in bridging the gap between idealized theoretical models and the complex reality of real materials. The intricate interplay of structural, electronic, and magnetic degrees of freedom in these materials often obscures the intrinsic properties of the Bi net itself.

In this study, we address this challenge by conducting a systematic investigation of Y_2O_2Bi single crystals using high-resolution angle-resolved photoemission spectroscopy (ARPES) and DFT calculations. Y_2O_2Bi, with its relatively simple electronic configuration, allows us to isolate the electronic contributions from the Bi square net, providing a "clean" system to study these 2D structures. Our study reveals a pronounced two-dimensional character of the Bi square lattice electronic states, confirming the effectiveness of the $[RE_2O_2]^{2+}$ layers in electronically decoupling the Bi square nets. Notably, we observe significant spin–orbit coupling effects on the band structure, particularly in the vicinity of the Fermi level. To further explore the influence of the chemical environment on the electronic structure and topological properties of the Bi square net, we perform DFT calculations for $SrMnBi_2$, $CaMnBi_2$, $LaPdBi_2$, and LiBi. These calculations reveal the potential for realizing topological phases in Bi square net systems, highlighting the importance of the surrounding crystal structure in dictating the electronic properties. This comparative approach provides a comprehensive understanding of the Bi square net and its potential for hosting novel quantum states.

2. Experimental and calculation methods

High-quality Y_2O_2Bi single crystals were synthesized via a self-flux technique. Elemental reagents were combined in an atomic ratio of $SrCO_3$:Y:Bi = 1:10:50. The reagents were placed in an Al_2O_3 crucible and sealed within an evacuated silica ampule. The samples were heated to 1100 °C at a rate of 150 °C/h, held for 50 hours, then cooled to 700 °C at a rate of 2 °C/h.

Synchrotron-based ARPES measurements were performed at beamline BL13U of the National Synchrotron Radiation Laboratory (NSRL) and beamline BL03U of the Shanghai Synchrotron Radiation Facility (SSRF). Samples were cleaved *in-situ* under ultra-high vacuum better than 5×10^{-11} Torr to ensure clean sample surfaces. Data acquisition was performed using a Scienta DA30-L electron energy analyzer, with a total energy resolution of 15 meV and an angular resolution of 0.2°. All ARPES data presented in this work were acquired using horizontally polarized light, which was empirically determined to provide optimal photoemission intensity for the relevant band features.

The bulk electronic structure calculations were performed in the framework of density functional theory (DFT) using the projector augmented wave method[30] as implemented in the Vienna *ab initio* simulation package.[31] The generalized gradient approximation of the Perdew–Burke–Ernzerhof type was adopted for the exchange–correlation functional. The cutoff energy was set to 450 eV and the Brillouin zone integration was performed on a Monkhorst–Pack k-point mesh of $8 \times 8 \times 5$ for Y_2O_2Bi, $11 \times 11 \times 5$ for $CaMnBi_2$ and $LaPdBi_2$, and $7 \times 7 \times 7$ for $SrMnBi_2$. The spin–orbit coupling effect was included in the first-principles calculations. The topological quantum chemistry (TQC) and magnetic topological quantum chemistry (MTQC) analyses were performed using the vasp2trace[32] and Mvasp2trace[33] codes through the Bilbao crystallographic server.

3. Results and discussion

Y_2O_2Bi crystallizes into a body-centered tetragonal structure ($I4/mmm$, No. 139) as illustrated in Fig. 1(a). The crystal structure consists of alternating layers of $[Y_2O_2]^{2+}$ and Bi^{2-}, with the Bi atoms forming a square lattice within each Bi layer. These $[Y_2O_2]^{2+}$ layers, with their formal positive charge, donate electrons to the Bi layers, effectively acting as charge reservoirs and influencing the electronic structure of the Bi square net. To clarify the nature of the interlayer bonding, we investigate the possibility of hybridization between Y and Bi atoms. The calculated shortest Y–Bi distance is 3.58 Å, significantly larger than typical covalent bond lengths in related compounds. This weak interaction is confirmed by electron localization function (ELF) calculations, as shown in Fig. 1(b), which reveal a clear ionic character with no significant covalent bonding path between the Y and Bi atoms. Furthermore, orbital-resolved band structure calculations confirm that the Y-d and Bi-p derived bands remain distinct and do not hybridize near the Fermi level. The layered structure promotes two-dimensional electronic behavior. Figure 1(c) shows the XRD pattern obtained from a platelike single crystal. All peaks can be indexed as (00l) reflections. Figure 1(d) illustrates the core-level photoemission spectrum, highlighting the characteristic Bi $5d_{3/2}$ and $5d_{5/2}$ peaks, accompanied by the bulk Brillouin zone of Y_2O_2Bi with clearly labeled high-symmetry points integrated into the image.

Figures 1(e) and 1(f) present the calculated electronic band structure of Y_2O_2Bi without and with SOC, respectively. Given the presence of the heavy element Bi, SOC plays a significant role in shaping the electronic structure. In the absence of SOC (Fig. 1(e)), the Bi $6p_x/6p_y$ and $6p_z$ orbitals contribute to distinct bands. However, when SOC is included (Fig. 1(f)), the band structure undergoes substantial modification due to

hybridization of the $6p_x/6p_y$ and $6p_z$ orbitals. This hybridization leads to the opening of band gaps on the order of hundreds of meV, particularly evident between -1.0 eV and -2.0 eV, indicating strong SOC-induced orbital mixing. It is important to note that, as Y_2O_2Bi possesses inversion symmetry, the bands remain spin-degenerate throughout the Brillouin zone. The observed splitting is therefore a result of lifted orbital degeneracy due to SOC, rather than a spin-splitting effect. Notably, as a result of SOC, a considerable number of $6p_x/6p_y$ electronic states shift downward toward the Fermi level (E_F) at the center of the Brillouin zone. This shift leads to a significant increase in the density of states (DOS) near the Fermi level, which is crucial for the electronic transport behavior of the Bi square net. Thus, the SOC-induced band splitting and hybridization are essential for understanding the electronic properties in the vicinity of the Fermi level. The bands around E_F are primarily derived from the Bi $6p_x/6p_y$ orbitals, which reside within the Bi square net plane, reinforcing the two-dimensional character of the electronic states.

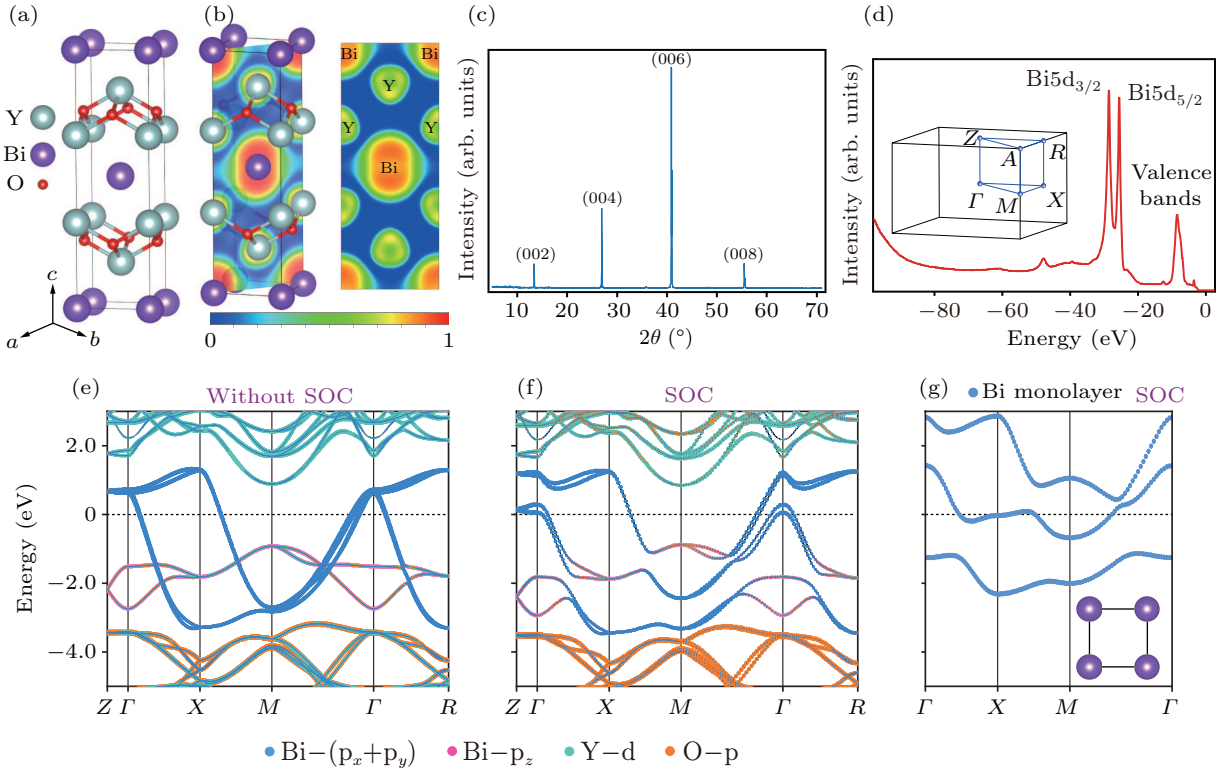


Fig. 1. Crystal structure, Brillouin zone, and characterization of Y_2O_2Bi. (a) Schematic crystal structure of Y_2O_2Bi, highlighting the Bi square net. (b) Calculated electron localization function (ELF) on the (110) plane. (c) Single-crystal x-ray diffraction pattern of Y_2O_2Bi showing (00l) reflections. (d) Core-level photoemission spectrum showing the characteristic Bi 5d peaks. The inset shows the bulk Brillouin zone of Y_2O_2Bi with labeled high-symmetry points. Calculated band structure of Y_2O_2Bi along high-symmetry directions without SOC (e) and with SOC (f), respectively. (g) DFT-calculated band structure of a monolayer Bi square net with SOC.

It is worth noting that this is significantly different from the Bi square net monolayer structure. The electronic structure of the Bi square net in Y_2O_2Bi exhibits profound differences from that of an isolated, neutral Bi square net monolayer, despite their structural similarities, as illustrated in Figs. 1(f) and 1(g). These differences arise primarily from two dominant effects. First, the Bi-derived bands in Y_2O_2Bi undergo a significant downward energy shift compared to those in the monolayer. This shift results from substantial charge transfer from the insulating $[Y_2O_2]^{2+}$ layers to the Bi square net, effectively rendering the Bi square net in Y_2O_2Bi a heavily electron-doped system. Consequently, the Fermi level is shifted deep into the conduction bands. Second, SOC manifests differently in the two systems. While the strong SOC of Bi atoms governs the band structure in both cases, its effects are modulated by the local environment. In the three-dimensional (3D) Y_2O_2Bi crystal, the Bi atoms experience a distinct crystalline potential and local symmetry compared to those in an isolated monolayer in a vacuum. This altered environment modifies the band dispersions and the magnitude of SOC-induced energy splitting. As a result, the pronounced band splitting in Y_2O_2Bi arises from a combination of intrinsic SOC and the specific 3D crystal field, rather than an enhancement of the SOC constant itself.

Figure 2(a) illustrates the DFT-calculated three-dimensional Fermi surface of Y_2O_2Bi. The Fermi surface is characterized by two columns (denoted as α and β) centered around M and Γ, respectively, exhibiting weak dispersion along the z-axis. This suggests predominantly two-dimensional electronic behavior within the xy plane. Fig-

ures 2(b) and 2(c) show the Fermi surface maps measured by ARPES using photon energies of 50 eV and 70 eV, respectively. The minimal change in the Fermi surface topology between these two photon energies strongly suggests the 2D nature of the electronic states in Y_2O_2Bi. First-principles calculations of the cleavage energy confirm that the energetically most favorable cleavage occurs between the Bi and $[Y_2O_2]^{2+}$ layers, naturally resulting in a Bi-terminated surface. The excellent agreement between the experimental and calculated Fermi surfaces for the Bi-terminated surface (Fig. 2(d)) strongly indicates that the ARPES measurements predominantly probe the electronic structure of the Bi square net. This further suggests that the Bi square net plays a dominant role in determining the low-energy electronic properties of Y_2O_2Bi. The weak photon-energy dependence of the electronic states near E_F, illustrated in Fig. 2(e), indicates minimal k_z dispersion, further supporting their 2D character. This is consistent with the DFT calculations, which show that these states are primarily derived from the Bi $6p_x/6p_y$ orbitals that lie within the plane of the Bi square net. For comparison, slab calculations were also performed for Y termination, Bi termination, and bulk projection, as shown in Figs. 2(f)–2(h).

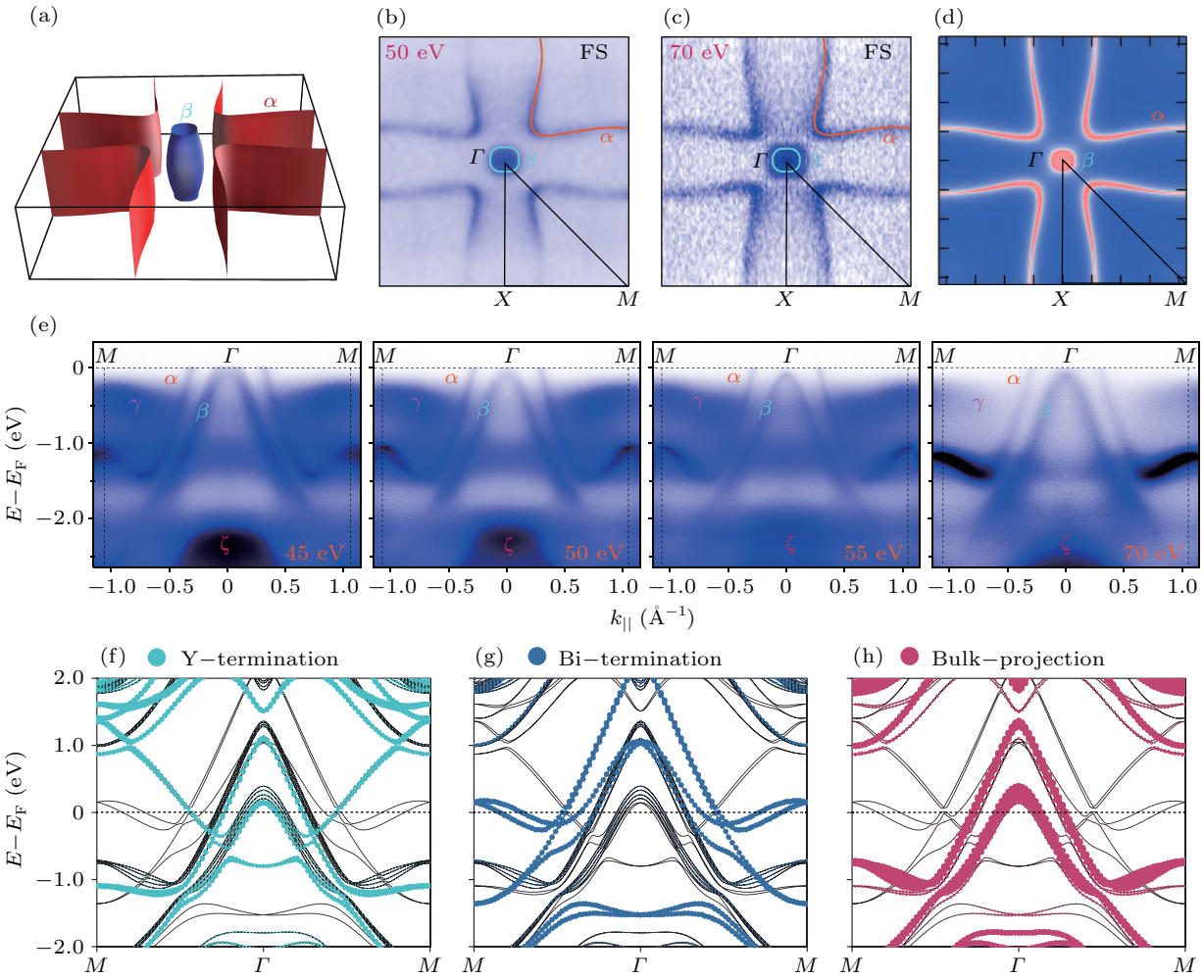


Fig. 2. Two-dimensional nature of the electronic structure of Y_2O_2Bi. (a) DFT-calculated three-dimensional Fermi surface. (b)–(c) ARPES-measured Fermi surfaces at photon energies of 50 eV (b) and 70 eV (c), respectively. (d) Calculated Fermi surface for the Bi-terminated surface. (e) ARPES-measured band dispersions along M–Γ–M at varying photon energies. Slab calculations for Y termination (f), Bi termination (g), and bulk projection (h), respectively.

Figure 3 compares the experimental ARPES results with calculations based on the surface Green's function method. ARPES intensity plots along the high-symmetry directions M–Γ–M, X–Γ–X, and M–X–M are shown in Figs. 3(a)–3(c), respectively. Within the ARPES spectra, we identify two distinct sets of bands: highly dispersive bands (α, β, ζ, and η) and less dispersive bands (γ and δ). A comparison of ARPES measurements with DFT calculations demonstrates that the observed highly dispersive bands (α, β, ζ, and η) are in excellent agreement with the calculated results for the bulk (Figs. 3(d)–3(f)) and the Bi-terminated surface (Figs. 3(g)–3(i)). In contrast, calculations for the Y-terminated surface reveal numerous surface states crossing E_F, a finding that significantly deviates from the band dispersion measured by ARPES (Figs. 3(j)–3(l)). The experimentally determined E_F is observed to be shifted upward by approximately 0.2 eV relative to the DFT calculations. This upward shift in the ARPES data suggests extra electron doping of the Bi square net, with $[Y_2O_2]^{2+}$ serv-

ing as an electron compensator.[34] The less dispersive bands γ and δ observed in the ARPES data are absent in the DFT calculations. Given that the primary Bi square net bands are clearly resolved, the most plausible origin of the ill-defined γ and δ bands is extrinsic states. It is important to consider the nature of the cleaved surface. The cleavage energy calculations indicate that the weakest bond is between the Bi and $[Y_2O_2]^{2+}$ layers (as shown in Fig. S1). Consequently, the cleavage process is expected to yield two complementary surfaces: one Bi-terminated and the other Y-terminated. While the excellent agreement between the main experimental bands (α, β, ζ, and η) and the calculations for the Bi-terminated surface confirms that this is the dominant termination probed in the experiment, it remains plausible that minority domains of the Y-terminated surface also exist on the sample. Given that the less dispersive γ and δ bands are not captured by calculations for the ideal Bi-terminated surface, we conclude that they are extrinsic in origin. A plausible explanation is that these features arise from surface imperfections, such as domains of the Y-terminated surface, defects such as Bi vacancies, or residual fragments from the cleavage process on either surface type. A definitive identification of the origin of these weak features would require further studies with microscopic surface probes.

The electronic structure of the Bi square net has been the subject of intense research, particularly regarding the possibility of hosting Dirac-like dispersions, as suggested by earlier theoretical studies on materials such as $CaMnBi_2$ and $SrMnBi_2$.[20] These materials incorporate Bi square nets as a structural motif. However, ARPES measurements and band

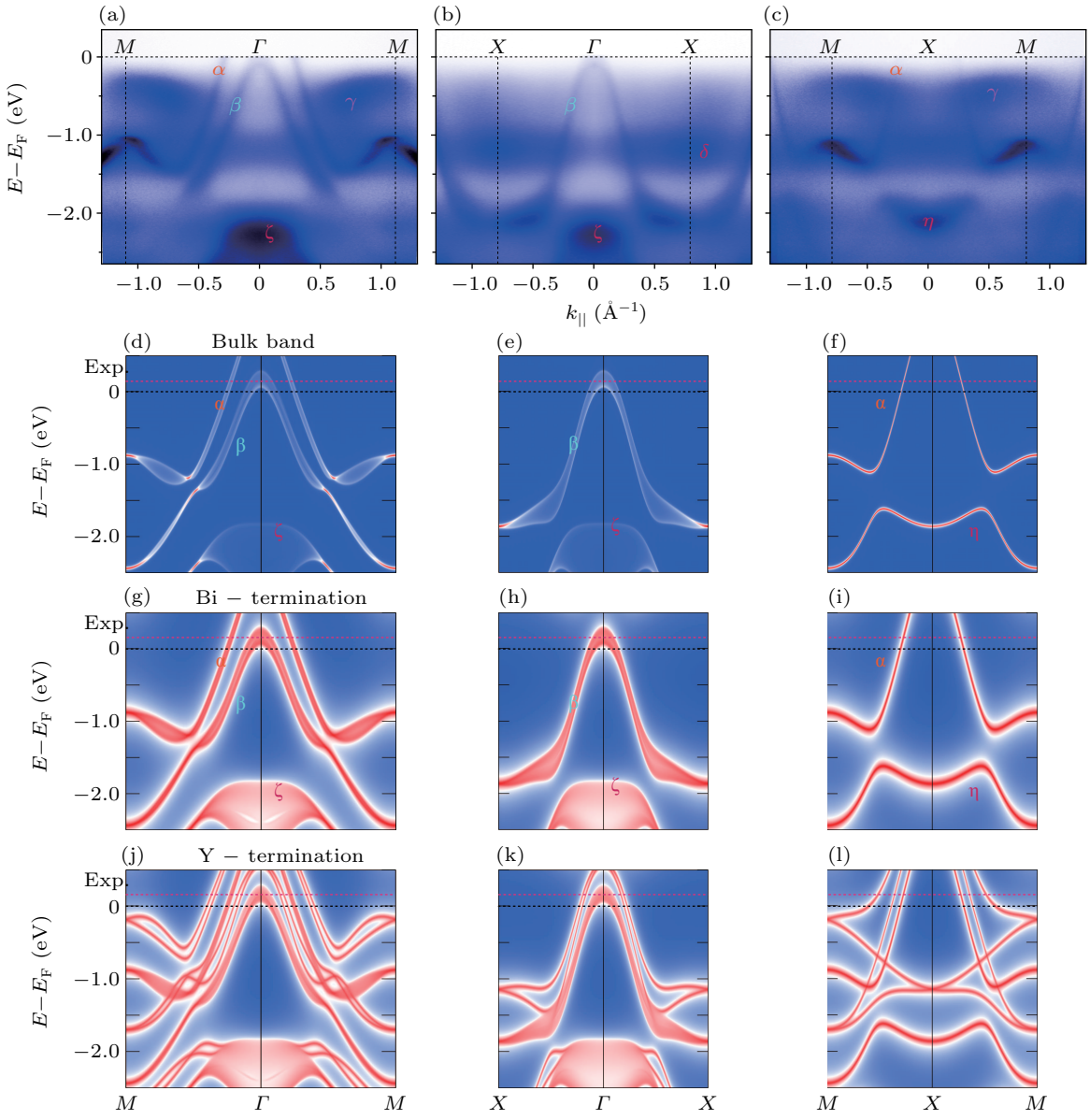


Fig. 3. ARPES measurements along high-symmetry lines compared with calculated band structures. ARPES-measured band dispersions along M–Γ–M (a), X–Γ–X (b), and M–X–M (c), respectively. DFT calculations employing the surface Green's function method yield the band dispersions for the bulk (d)–(f), Bi-terminated surface (g)–(i), and Y-terminated surface (j)–(l), respectively. The red dashed lines indicate the experimental E_F.

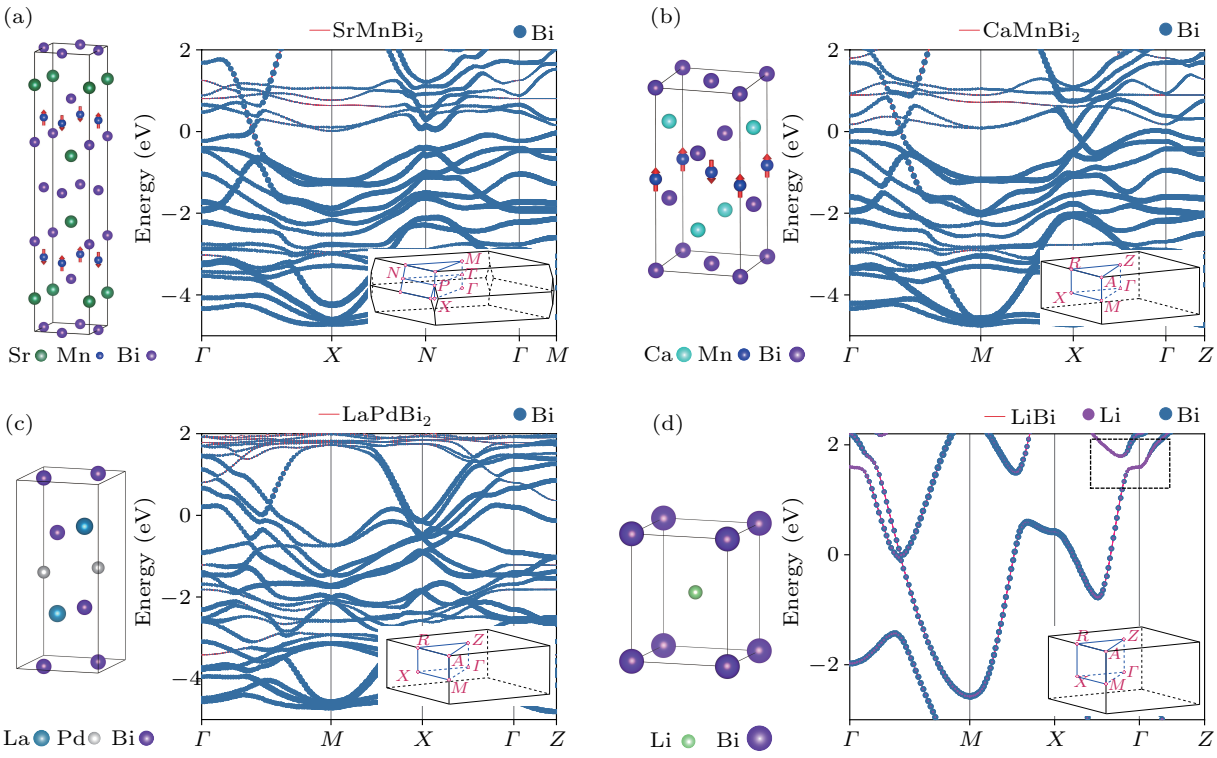


Fig. 4. DFT-calculated band structures of selected compounds containing Bi square nets. (a) $SrMnBi_2$ (magnetic space group $I4'/m'm'm$, No. 139.536), featuring 54 valence electrons. (b) $CaMnBi_2$ (magnetic space group $P4'/n'm'm$, No. 129.416), featuring 50 valence electrons. (c) $LaPdBi_2$ (space group $P4/nmm$, No. 129), featuring 62 valence electrons. (d) LiBi (space group $P4/mmm$, No. 123), featuring 6 valence electrons; the black dashed box indicates the band inversion.

calculations for Y_2O_2Bi demonstrate that a pristine Bi square net does not inherently possess topological band features. The presence of Mn and its magnetic ordering, along with the specific structural symmetries introduced by other elements, can significantly alter the electronic structure of the Bi square net compared to that in Y_2O_2Bi, potentially leading to the emergence of topological phases.

To investigate the influence of the surrounding crystal environment on the potential topological properties of the Bi square net, we performed DFT calculations and topological analyses for four materials containing Bi square nets, as illustrated in Fig. 4. We employed TQC and MTQC methods to analyze their topological properties. Our analysis reveals that three of these structures ($SrMnBi_2$, $CaMnBi_2$, and $LaPdBi_2$ (Figs. 4(a)–4(c))) exhibit trivial topological properties, despite the presence of prominent linearly dispersing bands reminiscent of Dirac cones. Previous studies suggested the presence of topological electronic states in these materials.[20,21,35,36] However, the present analysis indicates that these earlier conclusions require revision. These Dirac-like band dispersions, while interesting, do not necessarily indicate non-trivial topology. Specifically, the bands lying below the Fermi level can be represented as linear combinations of elementary band representations, indicating a lack of non-trivial topological characteristics.

Interestingly, calculations for LiBi (Fig. 4(d)), which also features a Bi square net, identify it as a topological insulator with a non-trivial $Z_4 = 3$ symmetry indicator.[37] This topological classification suggests the presence of protected surface states. This non-trivial topology is driven by hybridization between Li and Bi orbitals. As the orbital-projected calculations in Fig. 4(d) explicitly show, a band inversion occurs at the Γ point, where bands of Li-s and Bi-p character are inverted. This hybridization-driven band inversion, highlighted by the dashed box, is the origin of the topological insulator state. This finding highlights the crucial role of the surrounding crystal environment and interlayer interactions in shaping the electronic structure and topological properties of materials containing Bi square nets. Further investigation, including ARPES measurements on LiBi, would be valuable for experimentally verifying the predicted topological properties. Moreover, exploring other materials with modified Bi square net environments, such as through chemical substitution or strain engineering, could provide further insights into the factors governing the emergence of topological phases in these systems. A systematic study correlating the crystal structure, electronic structure, and topological properties across a wider range of Bi square net-based materials would be highly beneficial for advancing our understanding of these intriguing systems.

4. Conclusion

Our combined ARPES and DFT study of Y_2O_2Bi single crystals reveals the quasi-two-dimensional nature of the electronic structure, dominated by the Bi square net. The excel-

lent agreement between the ARPES-measured Fermi surface and the calculated Fermi surface for the Bi-terminated surface highlights the dominant role of the Bi square net in determining the low-energy electronic properties. Spin–orbit coupling leads to a significant band splitting and hybridization of the Bi 6p orbitals, and drastically enhances the density of states near the Fermi level. While Y_2O_2Bi itself is topologically trivial, the analysis of related Bi square net compounds demonstrates that the surrounding crystal environment can induce non-trivial topology. Specifically, while $SrMnBi_2$, $CaMnBi_2$, and $LaPdBi_2$ were found to be topologically trivial, LiBi exhibits the characteristics of a topological insulator.

Acknowledgments

This project was supported by the National Natural Science Foundation of China (Grant No. U2032153), the Strategic Priority Research Program of the Chinese Academy of Sciences (Grant No. XDB25000000), the Innovation Program for Quantum Science and Technology (Grant No. 2021ZD0302802), the Users with Excellence Program of Hefei Science Center of the Chinese Academy of Sciences (Grant No. 2021HSC-UE004), and the Fundamental Research Funds for the Central Universities (Grant No. WK2310000104). Numerical computations were performed at the Hefei Advanced Computing Center.

References

[1] Basov D, Averitt R and Hsieh D 2017 *Nat. Mater.* **16** 1077
[2] Tokura Y, Kawasaki M and Nagaosa N 2017 *Nat. Phys.* **13** 1056
[3] Keimer B and Moore J 2017 *Nat. Phys.* **13** 1045
[4] Chen X Z, Wang L, Zhang S, Zhang R J, Cheng Y W, Hu Y D, Meng C N, Liu Z T, Lv B Q and Huang Y B 2024 *Chin. Phys. B* **33** 087402
[5] Yu S, Wu X, Wang Y, Guo X and Tong L 2017 *Adv. Mater.* **29** 1606128
[6] Schaibley J R, Yu H, Clark G, Rivera P, Ross J S, Seyler K L, Yao W and Xu X 2016 *Nat. Rev. Mater.* **1**
[7] Novoselov K S, Mishchenko A, Carvalho A and Castro Neto A 2016 *Science* **353** aac9439
[8] Mannix A J, Kiraly B, Hersam M C and Guisinger N P 2017 *Nat. Rev. Chem.* **1** 0014
[9] Liu X and Hersam M C 2019 *Nat. Rev. Mater.* **4** 669
[10] Gupta A, Sakthivel T and Seal S 2015 *Prog. Mater. Sci.* **73** 44
[11] Glavin N R, Rao R, Varshney V, Bianco E, Apte A, Roy A, Ringe E and Ajayan P M 2020 *Adv. Mater.* **32** 1904302
[12] Ahn E C 2020 *npj 2D Mater. Appl.* **4** 17
[13] Wang Z, Dong H, Zhou W, Cheng Z and Wang S 2023 *Chin. Phys. B* **32** 067103
[14] Zhu H, Li T, Yu F, Li Y, Wang S, Wu Y, Liu Z, Shang Z, Cui S, Liu Y, Zhang G, Zhang L, Wang Z, Wu T, Ying J, Chen X and Sun Z 2023 *Chin. Phys. Lett.* **40** 047301
[15] Tremel W and Hoffmann R 1987 *J. Am. Chem. Soc.* **109** 124
[16] Schoop L M, Ali M N, Straßer C, Topp A, Varykhalov A, Marchenko D, Duppel V, Parkin S S, Lotsch B V and Ast C R 2016 *Nat. Commun.* **7** 11696
[17] Han F, Malliakas C D, Stoumpos C C, Sturza M, Claus H, Chung D Y and Kanatzidis M G 2013 *Phys. Rev. B* **88** 144511
[18] Kawasoko H and Fukumura T 2022 *Iscience* **25** 104742
[19] Mizoguchi H and Hosono H 2011 *J. Am. Chem. Soc.* **133** 2394
[20] Zhang A, Liu C, Yi C, Zhao G, Xia T L, Ji J, Shi Y, Yu R, Wang X and Chen C 2016 *Nat. Commun.* **7** 13833
[21] Guo Y, Princep A, Zhang X, Manuel P, Khalyavin D, Mazin I, Shi Y and Boothroyd A 2014 *Phys. Rev. B* **90** 075120
[22] May A F, McGuire M A and Sales B C 2014 *Phys. Rev. B* **90** 075109
[23] Mizoguchi H, Matsuishi S, Hirano M, Tachibana M, Takayama-Muromachi E, Kawaji H and Hosono H 2011 *Phys. Rev. Lett.* **106** 057002
[24] Sei R, Kawasoko H, Matsumoto K, Arimitsu M, Terakado K, Oka D, Fukuda S, Kimura N, Kasai H, Nishibori E, Ohoyama K, Hoshikawa A, Ishigaki T, Hasegawa T and Fukumura T 2020 *Dalton Trans.* **49** 3321
[25] Sei R, Kitani S, Fukumura T, Kawaji H and Hasegawa T 2016 *J. Am. Chem. Soc.* **138** 11085
[26] Terakado K, Sei R, Kawasoko H, Koretsune T, Oka D, Hasegawa T and Fukumura T 2018 *Inorg. Chem.* **57** 10587
[27] Qiao L, Wu N H, Li T, Wu S, Zhang Z, Li M, Ma J, Lv B, Li Y, Xu C, Tao Q, Cao C, Cao G H and Xu Z A 2021 *Front. Phys.* **16** 63501
[28] Cheng X, Gordon E E, Whangbo M H and Deng S 2017 *Angew. Chem., Int. Ed.* **56** 10123
[29] Kim H, Kang C J, Kim K, Shim J and Min B 2016 *Phys. Rev. B* **93** 125116
[30] Blöchl P E 1994 *Phys. Rev. B* **50** 17953
[31] Kresse G and Furthmüller J 1996 *Phys. Rev. B* **54** 11169
[32] Vergniory M, Elcoro L, Felser C, Regnault N, Bernevig B A and Wang Z 2019 *Nature* **566** 480
[33] Xu Y, Elcoro L, Song Z D, Wieder B J, Vergniory M G, Regnault N, Chen Y, Felser C and Bernevig B A 2020 *Nature* **586** 702
[34] Chen X, Deng J, Jin S, Ying T, Fei G, Ren H, Yang Y, Ma K, Yang M and Wang J 2023 *J. Am. Chem. Soc.* **145** 17435
[35] Park J, Lee G, Wolff-Fabris F, Koh Y, Eom M, Kim Y K, Farhan M, Jo Y, Kim C and Shim J 2011 *Phys. Rev. Lett.* **107** 126402
[36] Ray S J and Alff L 2017 *Phys. Status Solidi B* **254** 1600163
[37] Song Z, Zhang T, Fang Z and Fang C 2018 *Nat. Commun.* **9** 3530